Taylor & Francis
Taylor & Francis Group

Vehicle System Dynamics
International Journal of Vehicle Mechanics and Mobility

ISSN: 0042-3114 (Print) 1744-5159 (Online) Journal homepage: https://www.tandfonline.com/loi/nvsd20

Analysis of the evolvement of contact wire wear irregularity in railway catenary based on historical data

Hongrui Wang, Alfredo Núñez, Zhigang Liu, Yang Song, Fuchuan Duan & Rolf Dollevoet

To cite this article: Hongrui Wang, Alfredo Núñez, Zhigang Liu, Yang Song, Fuchuan Duan & Rolf Dollevoet (2018) Analysis of the evolvement of contact wire wear irregularity in railway catenary based on historical data, Vehicle System Dynamics, 56:8, 1207-1232, DOI: 10.1080/00423114.2017.1408919

To link to this article: https://doi.org/10.1080/00423114.2017.1408919

VEHICLE SYSTEM DYNAMICS
2018, VOL. 56, NO. 8, 1207–1232
https://doi.org/10.1080/00423114.2017.1408919

Analysis of the evolvement of contact wire wear irregularity in railway catenary based on historical data

Hongrui Wang [a,b], Alfredo Núñez[a], Zhigang Liu[b], Yang Song [b], Fuchuan Duan[b] and Rolf Dollevoet[a]

[a]Section of Railway Engineering, Delft University of Technology, Delft, Netherlands; [b]School of Electrical Engineering, Southwest Jiaotong University, Chengdu, People's Republic of China

ABSTRACT

This paper studies the evolvement of the wear irregularity of contact wire using wire thickness data measured yearly from a section of railway catenary. The power spectral density and time–frequency representation based on the wavelet transform are employed for data analysis, with an emphasis on local wear irregularities that are crucial for contact wire condition assessment. To investigate the cause of wear irregularity evolvement and the mutual influence with the pantograph–catenary dynamic interaction, simulations considering the influence of wear irregularity are carried out based on the finite element method. Analyses of the actual wear irregularities and the dynamic contact force under singular and complex wear irregularities are performed. Although the wear irregularity has limited impact on the pantograph–catenary interaction, it can induce the vibration of pantograph and contact wire that will lead to a notable increase of contact force standard deviation. The evolvement of wear irregularity is closely associated with the span length and dropper distribution of catenary structure and the running direction of pantograph. In addition, it is found feasible to detect the wear irregularity based on contact force, on condition that the sampling frequency is high enough to reflect the indicative frequencies.

ARTICLE HISTORY
Received 1 June 2017
Revised 9 October 2017
Accepted 16 November 2017

KEYWORDS
Railway catenary; wear irregularity; historical data; evolvement and cause; wavelet transform; finite element method

1. Introduction

With the massive construction of railway infrastructure and continuous upgrade of high-speed railway lines all over the world, various problems emerge intensively in operation and maintenance. For the power transmission of electrified railway industry, the overhead contact line system, namely the catenary system is the dominantly adopted subsystem. As the train runs through, the pantograph mounted on the train roof collects current from the catenary through the sliding contact with contact wire. During the process, the catenary system suffers impact from the pantograph, leading to the vibration of contact wire and the fluctuation in pantograph–catenary contact force. This brings problems for maintaining the quality of current collection and the stability of train operation. In The Netherlands, more than 327 operation disruptions are recorded as the results of defected catenary since

CONTACT Hongrui Wang soul_wang0@163.com

2011. Among all causes of disruption, the defected catenary usually requires the maximum average duration to recover [1,2], because of the difficulty of maintenance operation at meters above the ground. Aiming at reducing the amount of disruptions caused by defected catenary and cost saving, researchers and engineers pay more attention on the health condition monitoring of catenary system. In particular, as a major geometric property of the catenary system, the contact wire irregularity (CWI) [3] or unevenness [4] directly affects the sliding contact between the contact strip and the contact wire. So far, the impacts of CWI on the pantograph–catenary interaction still remain ambiguous whether and to what degree it is good or bad for current collection. Moreover, these impacts are likely to be amplified under high speeds, resulting in contact loss, arcing, severe wear, etc. that impair the current collecting quality and the service life of catenary system. Thus, aiming at improving the performance of catenary system, the concept of CWI has been drawn more and more attentions in recent years [3–9].

CWI is the result of all factors that deviates the spatial position of the lower surface of contact wire from the nominal position. Since CWI is mainly caused from the manufacture, installation and wear of the contact wire, it can be regarded as an inevitable existence in any soft catenary system in reality [5]. Some other random environmental factors such as wind, temperature, icing and so on can also cause and change the irregularity under certain circumstances. Generally speaking, the combination of the geometry deformation and the lower surface unevenness of contact wire together constitute the CWI. While the causes of the geometry deformation can be much complex in practice, the causes of the lower surface unevenness mainly include the manufacturing defect, sliding wear and electric corrosion of contact wire [6]. In previous studies, some experiments and simulations are carried out to investigate the influence of CWI on pantograph–catenary interaction [6–9]. However, due to the difficulties in measurement and data analysis, some sporadic conclusions are obtained concerning the local singularity and distributed irregularity of contact wire. Because the local singularity can induce an instantaneous impact on both pantograph and catenary, its acceptable level of amplitude is sensitive to the operation speed and pantograph type [6,7]. Normally, the requirement will be higher if the operation speed is faster. For the distributed irregularity, the irregularity wavelength is considered to be crucial for the influences on pantograph–catenary interaction [7,8]. Instead of treating the CWI as a whole, the geometry deformation and lower surface unevenness can also be studied separately [9] considering their different cause and level of magnitude. But above all, the influence of CWI on pantograph–catenary interaction has not yet been fully revealed. The effects of various irregularities on the pantograph–catenary contact force still requires intensive study to understand if they are actually favourable or unfavourable for current collection. It is the premise for maintenance decision making so that catenary systems can be maintained under an acceptable condition for long-term normal operations while reducing overall cost.

This paper focuses on the lower surface unevenness of contact wire, namely the wear irregularity that can be described by the contact wire thickness from in-situ measurements. It not only influences the current collection quality, especially when the train speed is higher than 200 km/h, but also correlates with the life cycle cost of contact wire. It is also believed to be one of the main reasons that cause wire breakages in extreme cases. Normally, if the wire thickness at a certain location is less than a default threshold, the corresponding wire must be replaced partially or integrally depending on the maintenance strategy.

The formation of contact wire wear is mainly determined by the material types of contact strip and contact wire, amplitude of contact force, current flow intensity and environmental factors. Accordingly, some methodologies and experiments are carried out to predict the contact wire wear [10,11], which can provide general predictions of contact wire wear rate under the influence of pantograph passages. To understand how the contact wire wear are formed under electric current, the wear mechanism between contact strip and contact wire are experimentally analysed in [12–15]. It is believed that the contact temperature induced by sliding friction and arcing determines the wear modes between contact strip and contact wire.

However, in daily operations, the contact wire suffers much complex loads that may be varying with every pantograph passage. For a section of contact wire at a certain location, the pantograph speed, arcing, temperature, wind, rainfall, and in some cases even the pantograph type are all variable factors that change constantly. Moreover, contact wires at various geographical locations face significant climate differences. Thus, the actual wear growth of contact wire is difficult to be fully simulated by mathematical models or experimental setups. But, with the help of historical measurement data, the evolvement of contact wire wear irregularity in term of wire thickness variation can be precisely acquired. Through analysing and grasping the pattern of wear irregularity in both time and frequency domains, the wear evolvement and the corresponding causes could be objectively observed and potentially explained. This can also be considered as the prior knowledge for the design of prognostics and health management for the catenary system. It provides references to achieve the preventive maintenances depending on prognostics rather than traditional diagnostics, thus leading to lower maintenance costs eventually.

Therefore, this paper aims to investigate the evolvement of contact wire wear irregularity based on historical data. To comprehensively obtain data features and the evolvement of features over time, the commonly used time-domain statistics including mean, standard deviation (SD) and extrema, and the power spectral density (PSD) estimation are adopted for feature extraction [16–18]. In addition, because the local CWIs possess limited spatial distance along the entire contact wire, they cannot be observed by PSDs in the frequency domain. Thus, the time–frequency analysis with information concerning the spatial position is employed [19,20]. Techniques such as short-time Fourier transform, quadratic time–frequency distributions and wavelet transform can transform signals into the time–frequency domain. Thus, the frequency deviations or emergences of signal can be observed with knowing the corresponding positions of occurrence. This effect is particularly practical for observing the degradation of local irregularity in both distance and frequency. Meanwhile, the distributed irregularity can also be recognised in the time–frequency domain with long distance intervals. Because the local irregularity of contact wire is important for condition assessment and thus maintenance decision making, the wavelet transform with the superiority in the singularity detection of signals [21] is utilised for the time–frequency analysis in this paper.

With all the observed evolvement patterns, their reasons of occurrence still need to be explained and associated with controllable elements in the catenary system. In practice, the direct cause of contact wire wear is undoubtedly the repetitive pantograph–catenary sliding contact. The contact force between pantograph and contact wire is directly proportional to the force of sliding friction. In undesirable cases, it gives rise to arcing if too low or induces severe wear if too high, through which eventually lead to observable wear

irregularities along the wire. Therefore, in order to understand the mutual effects of wire wear and pantograph–catenary contact force on each other, it is necessary to employ a numerical model to simulate the pantograph–catenary dynamic interaction under wear irregularities of contact wire. In this way, influences of different degrees of wear irregularity on the current collection quality can be obtained, which can facilitate the decision making of necessary maintenance actions. Moreover, concerning the upgrade of maintenance strategy, the feasibility of using contact force as an indicator for wear irregularity diagnosis [22] or prognosis is investigated as well.

The rest of this paper firstly analyses the wear irregularity of contact wire from measurements and then studies its mutual influence with the pantograph–catenary interaction through simulations. Concretely, some basic information about the measurement data of contact wire thickness is given in Section 2. The adopted PSD estimation and time–frequency analysis methods are introduced in Section 3 and applied to the measurement data in Section 4. Section 5 presents the simulation of pantograph–catenary interaction under the contact wire wear irregularity from measurements. Section 6 discusses the evolvement of wear irregularity combining both measurement and simulation results. Finally, some conclusions are drawn in Section 7.

2. Measurement data description

The data employed in this paper are measured from a railway line that operates daily in The Netherlands. For condition-based monitoring of the catenary, the contact wire thickness, with a nominal value of 12 mm is inspected regularly. The spatial positions of sampling points are obtained simultaneously based on the GPS device installed on the measurement coach. Since the measurements are carried out on a yearly basis, the evolvement of contact wire thickness can be observed corresponding to the same spatial positions. The sampling rate is a fixed interval of 0.5 m. The measured two types of wire thickness are described as follows.

(1) Contact wire average thickness that is the average vertical thickness of contact wire profile in every sampling interval.
(2) Contact wire minimum thickness that is the minimum vertical thickness of contact wire profile in every sampling interval.

The measurement resolution of wire thicknesses is 0.1 mm, which is equal to the suggested minimum resolution for CWI measurements [4]. Since the wire thickness is measured one year apart and sampled at a fixed interval, it cannot be guaranteed that the sampling point is from precisely the same position for every year. But, to compute the average in a 0.5 m interval should somehow mitigate this minor deviation in position. In cases of severe local wear that could be overlooked by the averaging, the minimum thickness in one interval can preserve their presences, as they are important for deciding if wire replacement or maintenance is required. Therefore, together the minimum and average thicknesses of contact wire can provide a comprehensive view of the growth of contact wire wear.

Figure 1 depicts a set of contact thickness data measured at the same section of railway line from year 1 to year 4, during which the contact wire had never been replaced nor

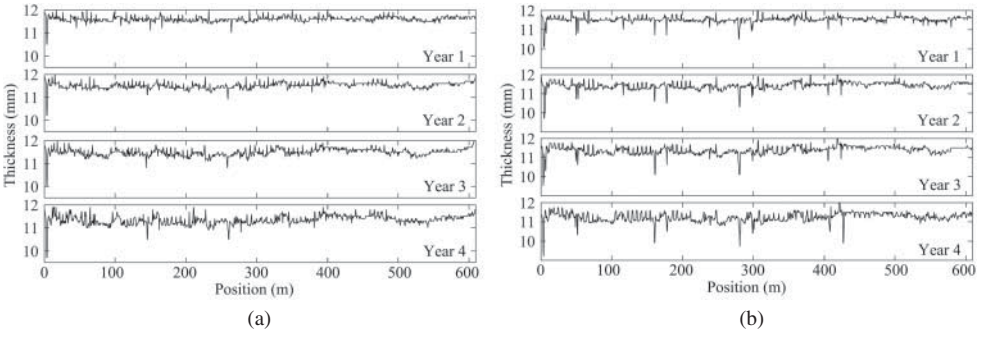

Figure 1. A set of contact wire thickness data (year 1 to year 4 from top to bottom). (a) Contact wire average thickness. (b) Contact wire minimum thickness.

maintained. It can be seen that the wear of contact wire is growing yearly, on the basis of the pattern that is already formed in the first measurement of year 1. Also, there is a severely worn sampling point near the beginning of this section of catenary and some others are only observable from the minimum thickness data. Figure 2 depicts the box plots of the two types of thickness with respect to time. According to the box plot of the average thickness data, the contact wire wear, in term of thickness loss, increases slowly by about 0.09 mm per year and becomes more unevenly distributed with the increasing dispersion. The minimum values of the average thickness, representing the severest worn section of contact wire, have a much more rapid decrease of about 0.27 mm per year. The similar trend can be found from the box plot of the minimum thickness data with smaller overall thickness and rapider decrease in thickness comparing with that of the average thickness. In addition, the outliers in the thickness data marked by the plus signs reflect the existences of some significant local irregularities. As a result, there are more local irregularities revealed

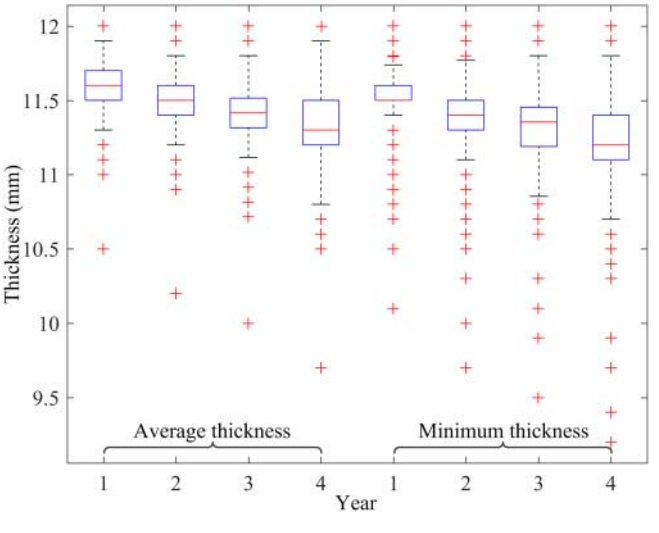

Figure 2. Box plot comparisons of evolvements of the average thickness and the minimum thickness.

by the minimum thickness than by the average thickness for obvious reasons. For a different railway line, the decrease rate of wire thickness varies proportionally with the traffic density of the line considering the number of pantograph passages per unit time.

3. Data analysis methods

3.1. PSD estimation

To analyse the frequency characteristics of catenary measurement data, the PSD estimation is frequently adopted. It is mainly used for analysing the dominant frequencies of CWI or contact force [6–9] that are intrinsic and constant depending on the structural parameters of catenary and pantograph. Although these measurement data might not be strictly time-invariant due to the existence of local CWI and other interferences, PSD by its nature can still extract the dominant frequencies while neglecting the time-variant components. Traditional PSD estimation methods are non-parametric and mostly based on the Fourier transform, including the periodogram method and the enhanced periodogram methods such as the Bartlett method and the Welch method [23]. For a discrete stochastic process with N data samples $\{x(n); n = 1, 2, \ldots, N\}$, the Fourier transform of the data set is

$$X(\omega) = \sum_{n=1}^{N} x(n)\mathrm{e}^{-\mathrm{i}\omega n}. \tag{1}$$

The PSD estimated by the periodogram is

$$P_x(\omega) = \frac{1}{N}|X(\omega)|^2. \tag{2}$$

However, even with several enhancements for the periodogram method, the non-parametric methods still suffer from the spectral leakage problem, which is inconvenient for the precise frequency identification of a physical signal. Thus, the parametric methods with high-frequency resolution are proposed. One of the well-known representatives is the autoregressive (AR) model estimation method [24]. The data series $x(n)$ can be described by the basic form of AR model

$$x(n) = \sum_{k=1}^{p} a_k x(n-k) + e_n, \tag{3}$$

where p is the order of AR model, a_k are the AR coefficients and e_n is a white noise process with zero mean and finite variance σ_e^2. The estimated PSD based on the AR model is

$$S(\omega) = \frac{\sigma_e^2}{\left|1 - \sum_{k=1}^{p} a_k \mathrm{e}^{-\mathrm{i}\omega k}\right|^2}, \tag{4}$$

where σ_w^2 and a_k can be calculated by solving the Yule–Walker equations [25].

In the AR model, the determination of order p is crucial for the precise representation of data set $x(n)$. If the order p is too high, the estimated PSD will deviate from the actual PSD and even generate false frequencies. If the order p too low, some true frequency components

may be submerged and become unobservable. To obtain the best order that fits a given data set with minimum information lost, there is one criterion frequently employed, namely the Akaike information criterion (AIC) [25]. It is computed by

$$\mathrm{AIC}(p, N) = N \ln \hat{\sigma}^2 + 2p, \tag{5}$$

where $\hat{\sigma}^2$ is the mean square of residuals defined as

$$\hat{\sigma}^2 = \frac{1}{N} \sum_{i=1}^{N} \hat{\varepsilon}_i^2 \tag{6}$$

and $\hat{\varepsilon}_i$ are the estimated residuals from the fitted model using least squares estimation. The order that results in the minimum criterion value is considered to be optimal for the AR model of the data set. To facilitate the comparison of AIC values, the normalised values can be calculated by

$$\mathrm{NAIC}(p, N) = \frac{\mathrm{AIC}(p, N) - \min(\mathrm{AIC})}{\max(\mathrm{AIC}) - \min(\mathrm{AIC})}, \tag{7}$$

where $\min(\cdot)$ and $\max(\cdot)$ denote the minimum and maximum criterion values among all the model orders under consideration. Taking the data set in Figure 1 as an example, Figure 3(a,b) depicts the normalised AIC criterion values of the average thickness and the minimum thickness respectively, considering the model order ranges from 1 to 50. It can be seen that the two types of thickness result in different optimal model order that varies from one year to another. Thus, it is necessary to properly determine the model order beforehand to avoid inaccurate PSD estimation. Then, the corresponding PSDs can be obtained

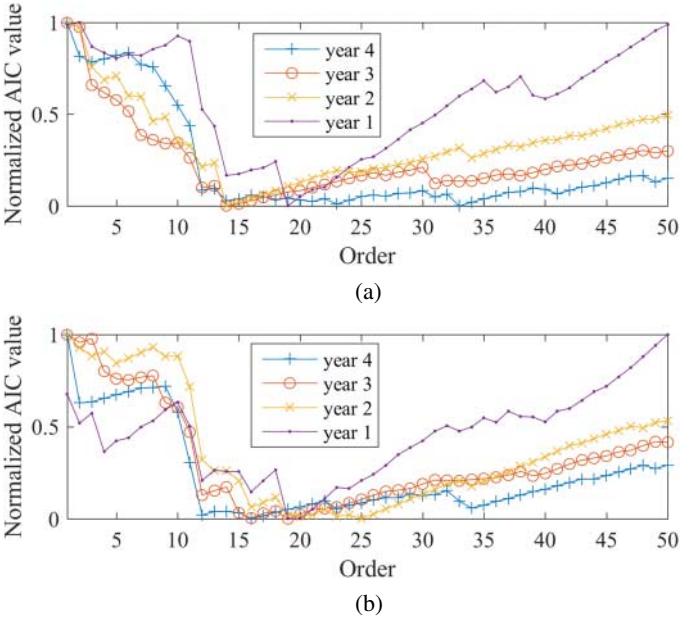

Figure 3. Comparisons of the normalised AIC value with respect to the model order for thickness data from different year. (a) Contact wire average thickness. (b) Contact wire minimum thickness.

by Equation (4). Hereafter, the order selection for every data series is realised by comparing the criterion values within orders from 1 to 100 to ensure accurate PSD estimations.

3.2. Time–frequency analysis

The time–frequency representation (TFR) of a signal is a three-dimensional representation that describes the energy distribution of the signal in the time–frequency plane. It has been widely used in engineering problems concerning the analysis of signals with varying frequency. In general, if a signal contains transient frequencies or its basic frequencies are changing with time, the time–frequency analysis can reveal the existence of these time-variant components while the PSD could not. Considering the contact wire wear with local irregularity or singularity caused by a hard point or arcing, the wire thickness data should have varying statistics along the longitudinal direction. This feature accords with the superiority of time–frequency analysis so that it can be fully represented.

Based on the fundamental Fourier transform, the basic time–frequency analysis, namely the short-time Fourier transform can be realised through multiplying the target signal by window functions with short duration before transformation. It utilises the multiple one-dimensional transformations to constitute a two-dimensional representation. However, the time and frequency resolutions of short-time Fourier transform are constrained by the uncertainty principle as a trade-off between each other. Consequently, the combined time–frequency resolution is limited in the resulting TFR. This becomes especially inconvenient for analysing the local irregularities in contact wire wear, as the length and position of local irregularity are likely to be distorted by the short-time Fourier transform. Addressing this issue, the TFR based on wavelet transform is frequently employed. Instead of using trigonometric functions as signal basis for signal decomposition, the wavelet transform utilises the mother wavelet that can shift and scale in time to fit the target signal, particularly for the local variation in signals. Thus, the TFR based on wavelet transform is proven to have a general higher resolution than the short-time Fourier transform. The wavelet coefficients from the data series $x(n)$ decomposed by wavelet transform are defined as [26]

$$W_x(u,s) = \sum_{n=1}^{N} x(n) \frac{1}{\sqrt{s}} \psi * \left(\frac{(n-u)\Delta t}{s} \right), \tag{8}$$

where Δt is the time interval of data series $x(n)$, * denotes complex conjugate, $\psi*$ is a family of wavelets deduced from the mother wavelet by translation and scaling operations, u and s are the translation and scale parameters, respectively, and $W_x(u,s)$ are the wavelet coefficients of data series $x(n)$. The corresponding TFR or the so-called scalogram is defined as

$$S_T(f) = |{W_x}^2(u,s)|, \tag{9}$$

where $S_T(f)$ is the wavelet-based power spectrum that indicates the frequency response in an interval of time or position T. For consistency, the following TFRs are computed choosing the Morlet function as the mother wavelet for wavelet transform. It should be noted that for both PSD and time–frequency analysis in the following, the mean value of each data series is removed beforehand to cancel its influences on frequency reflection. This is to achieve a better frequency extraction results without the interferences of the overall energy level.

4. Data analysis of wear irregularity

If necessary, regular maintenances normally adjust the contact wire height to meet the general requirement of pantograph–catenary contact. Little maintenance can be done specifically to control the growth of wear irregularity. The wear irregularity of contact wire is constantly evolving with the everyday operation until replacements. As discussed above, the average wear of contact wire is normally growing slower comparing with the local wear with higher thickness loss. However, replacements of contact wire are mostly depending on these thin spots, where wire breakages are likely to happen, regardless of the overall wear rate. Thus, additional attentions are paid to the severe local wear in the data analysis of contact wire wear irregularity. Based on the aforementioned methods, some frequency characteristics of the contact wire wear irregularity can be obtained.

Figure 4(a,b) depicts the PSDs of the average thickness and the minimum thickness, respectively. By identifying the minimum criterion value presented in Figure 3, the selected AR model order for the contact wire average thickness from year 1 to year 4 are respectively 19, 14, 14, and 33, and for the minimum thickness from year 1 to year 4 are respectively 19, 20, 19, and 12. For both types of thickness, the overall spectral density is increasing every year with the cumulative thickness loss. The trend and peaks of the PSDs are all similar, but among which the PSDs of the minimum thickness appear to be more smooth and consistent. In particular, there are two frequency peaks standing out and observably raising with the year. As indicated in the figures, for the average thickness and the minimum thickness, the highest peaks are locating at the spatial frequency of 0.178 and 0.172 m^{-1}, respectively. They are equivalent to the wavelength of 5.6 and 5.8 m, approximately representing the distance between droppers that are consistently about 5.5 m. This can be

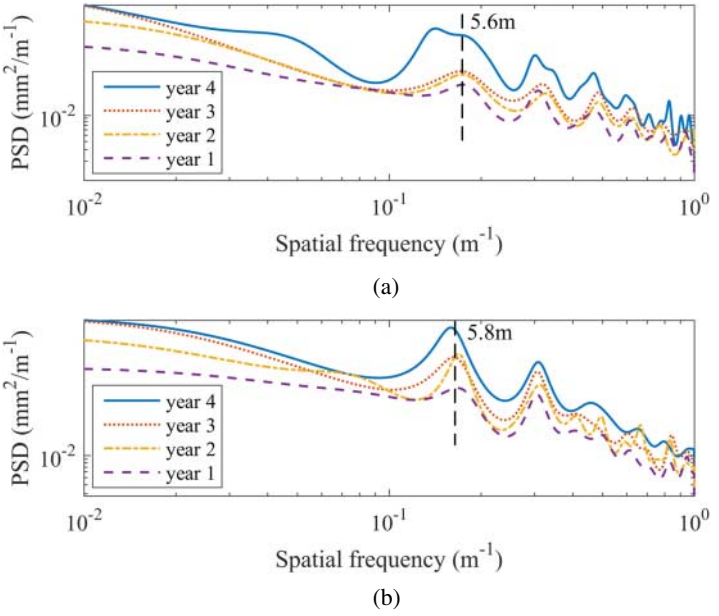

Figure 4. Comparisons of PSDs of the thickness data from different year. (a) Contact wire average thickness. (b) Contact wire minimum thickness.

considered as the effect of repetitive sliding friction force exerting on the contact wire surface, which is directly proportional to the amplitude of pantograph–catenary contact force. Due to the variation of stiffness along the contact wire attributed to the existence of droppers, the contact force contains the wavelength induced by the placement of droppers [27]. Thus, it introduces the wavelength into the friction force that eventually results in this frequency feature of contact wire wear. Including analyses on other data that are not shown in this paper, this wavelength is highly consistent and invariable.

From another perspective, Figure 5(a,b) depict the TFRs of the average thickness and the minimum thickness based on wavelet transform, respectively. Since the mean of each data series is removed, the overall power in terms of wavelet coefficient for both types of thickness is actually increasing because the yearly growth of thickness loss is uneven. From Figure 5(a), it can be seen that the growth of wear irregularity appears mainly in three regions that are circled by dashed lines and numbered as region 1, 2 and 3 in the TFRs. The region 1 is at the beginning of the data interval with a wide frequency range centralised around the spatial frequency 0.17 m^{-1}, which is equivalent to the wavelength of inter-dropper distance. It agrees with the frequency peaks in the PSDs and indicates the

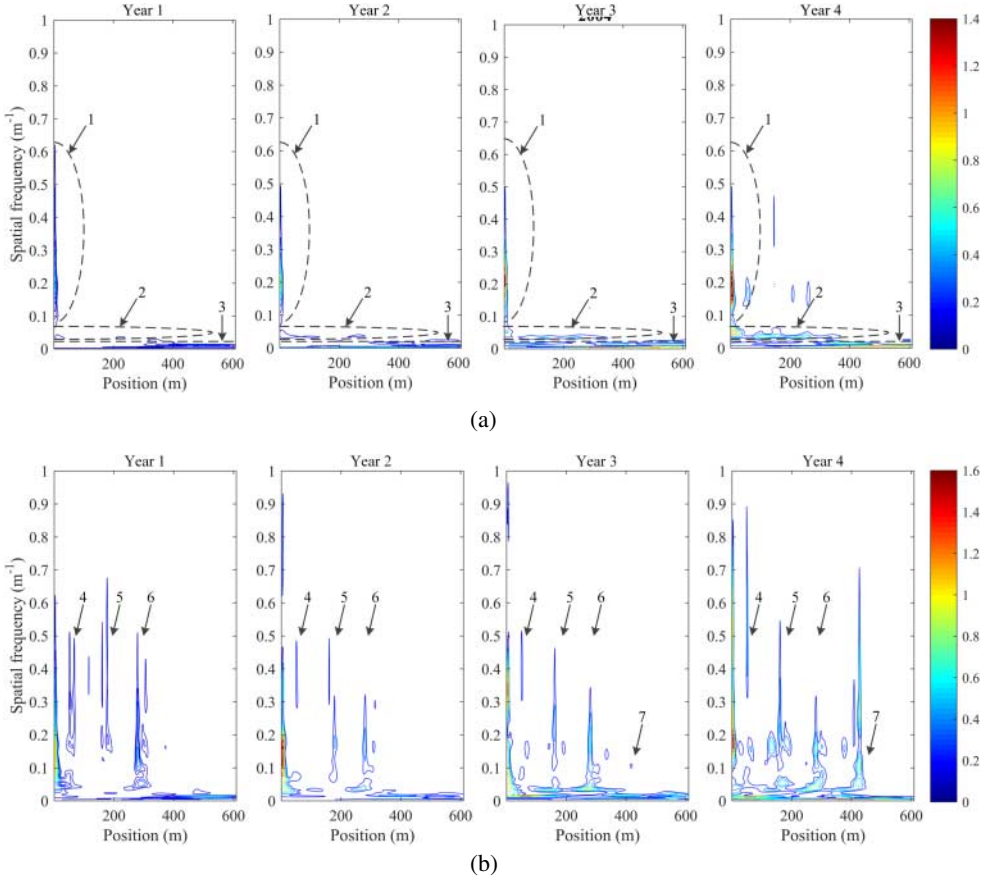

Figure 5. Comparisons of TFRs of the thickness data from different years. (a) Contact wire average thickness. (b) Contact wire minimum thickness.

severe local wear at the same position as shown in Figure 1(a). The region 2 is located at the low-frequency range below 0.02 m^{-1} throughout the entire contact wire. It indicates the increasing overall level of wear irregularity related to the long wavelength of spans. The region 3 indicates emerging frequencies that initially appear in year 1 around 0.034 m^{-1} in spatial frequency, which is about 30 m in wavelength related to half a span or five times of inter-dropper distance. Then, it becomes more severe with time and expands along the contact wire until reaching 380 m in position in year 4. Meanwhile, the same type of severe local wear emerges in year 4 at the same frequency range around 0.17 m^{-1} as the region 1 mentioned before. These emerging local irregularities are reflected more clearly in the TFRs of minimum thickness in Figure 5(b). It can be seen that, aside from the region 1 2 and 3 in the case of average thickness, there are three local irregularities revealed in year 1 and located at around 61, 181 and 298 m in position, respectively. They are marked as region 4, 5 and 6 in Figure 5(b). They are constantly growing in power and associated with irregularities that are also growing around 0.034 m^{-1}. In year 3 and 4, another similar local irregularity marked as region 7 appears at around 424 m with the same pattern as the region 4, 5 and 6. The four local irregularities are at a distance of approximate 2 spans, as a result of the high-amplitude contact force around the location where the pantograph passes the contact wire regulated by registration arms.

Combining analyses on both the TFRs of average and minimum thicknesses, it can be found that there is a directional property for the evolvement of contact wire wear irregularity. As the actual running direction of trains is from 0 to 600 m in position, the wear irregularity is increasing in the same direction with the emerging distributed irregularity identified around 0.034 m^{-1} and local irregularities identified around 0.17 m^{-1}. While the location and frequency of these emerging irregularities can be associated with the wavelengths attributed to the catenary structure, this directional property implies that the growth of wear irregularity is also influenced by those pre-existing irregularities, in this case the local wear at the beginning of the contact wire interval. Therefore, influences of contact wire wear irregularity on the pantograph–catenary interaction can help explaining these patterns of evolvement and facilitate the control of wear irregularity.

5. Pantograph–catenary interaction simulation with wear irregularity

5.1. Simulation of pantograph–catenary interaction

The simulation technique of pantograph–catenary interaction is well developed in the past years and comprehensively summarised in [28]. At present, the finite element method (FEM) is the dominant technique in pantograph–catenary dynamic simulation. In this paper, the pantograph–catenary interaction is modelled by combining the catenary model based on cable and truss elements and the basic three-lumped mass model of pantograph [29]. In the catenary model, the contact wire and messenger wire are modelled by nonlinear cable elements, and the droppers are modelled by nonlinear truss elements. Firstly, the initial configuration of catenary model is obtained by the shape-finding method that is verified by several numerical examples. Then, to solve the dynamic response of catenary under a moving load, a structural dynamic equation is formed as

$$\mathbf{M}\Delta\ddot{\mathbf{X}}(t)+C\Delta\dot{\mathbf{X}}(t)+\mathbf{K}(t)\Delta\mathbf{X}(t)=\Delta\mathbf{F}(x,t), \tag{10}$$

where $\Delta\ddot{\mathbf{X}}(t)$, $\Delta\dot{\mathbf{X}}(t)$ and $\Delta\mathbf{X}(t)$ are the incremental vectors of the global acceleration, velocity and displacement for the catenary, respectively. $\mathbf{M}$ and $\mathbf{C}$ are the global lumped mass matrix and the global damping matrix, which are considered constant during the simulation. The global stiffness matrix $\mathbf{K}(t)$ of the catenary is formulated through the FEM at time instant t. $\Delta\mathbf{F}(x,t)$ is the incremental vector of the excitation at position x, which includes the PCCF exerted on the contact point and the internal force of catenary structure.

The PCCF is the connection between the catenary model and the three-lumped-mass pantograph model depicted in Figure 6, which is composed of three lumped masses and three spring-damper elements. The dynamic response of pantograph can be described as

$$\begin{aligned} &m_1\ddot{y}_1 + c_1(\dot{y}_1 - \dot{y}_2) + k_1(y_1 - y_2) = -F_c(x,t) \\ &m_2\ddot{y}_2 + c_1(\dot{y}_2 - \dot{y}_1) + c_2(\dot{y}_2 - \dot{y}_3) + k_1(y_2 - y_1) + k_2(y_2 - y_3) = 0 \\ &m_3\ddot{y}_3 + c_2(\dot{y}_3 - \dot{y}_2) + c_3\dot{y}_3 + k_2(y_3 - y_2) + k_3y_3 = F_u, \end{aligned} \tag{11}$$

where $F_c(x,t)$ is the dynamic contact force exerting on the pantograph, F_u is the uplifting force of pantograph, and y_1, y_2 and y_3 are the vertical displacements of the three lumped masses.

Finally, the pantograph–catenary contact force is calculated by the frequently adopted penalty function based on the penetration depth and the contact stiffness K_c between the contact wire and the pantograph as follows.

$$\begin{aligned} &F_c(x,t) = K_c(u_p(t) - u_c(t)) \quad u_p(t) \geq u_c(t) \\ &F_c(x,t) = 0 \quad u_p(t) < u_c(t), \end{aligned} \tag{12}$$

where $u_p(t)$ and $u_c(t)$ are vertical positions of the pantograph and the contact wire at the time instant, respectively. During the interaction, the aerodynamic force exerting on the pantograph head is considered based on an empirical equation

$$F_a = 0.00095v^2 + 0.0017v - 0.2, \tag{13}$$

where v is the speed of pantograph in the unit m/s. The total uplifting force of pantograph F_u is the sum of the aerodynamic force F_a and the initial contact force that is 140 N in the case of Dutch conventional lines. The above pantograph–catenary modelling

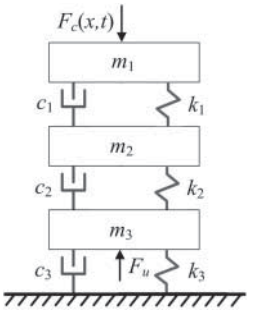

Figure 6. The three-lumped mass model of pantograph.

approach has been verified by both the recent benchmark presented in [28] and the EN 50318 standard [30].

The current standard and benchmark specify the validation of pantograph–catenary simulation based on statistics of simulation data at the frequency range below 20 Hz. However, this paper intends to analyse the information contained in the simulation data at the range above 20 Hz. It is thus necessary to validate the model at a high-frequency range. To this end, the model validation is carried out by comparing the mean and PSD of contact forces when the simulation parameters including contact stiffness, element length and sampling time are different. The selected values of the three parameters for model validation are listed in Table 1. Some related parameters for the pantograph–catenary dynamic simulations in this paper are also given. Parameters that are not specified in the table, including those of pantograph and the material properties of contact wire, messenger and dropper, are selected as in the benchmark model in [28] due to the unavailability of these parameters. While this might not be favourable for the simulation results comparing with using real-life parameters, it should be noted that this paper mainly discusses the relationship between the catenary geometrical shape concerning the clamping points on contact wire and the wear irregularity of contact wire.

For the model validation and further simulations, the catenary model has a unified structure of 14 spans. The dynamic simulation results from the two spans at both ends of the catenary structure are abandoned due to the severe influence of boundary effect. The results for model validation at high frequencies are depicted in Figure 7. The mean of contact force that is not low-pass filtered are depicted in Figure 7(a–c), corresponding to the change of the three parameters respectively. It can be seen that the mean contact forces vary slightly with the change of parameters, resulting in a maximum variation of 0.88‰, 0.86‰ and 0.28‰ comparing with the case of the employed values for further simulations. Similarly, comparisons of the PSDs of contact forces are depicted in Figure 7(d–f) corresponding to the change of the three parameters respectively. It can be seen from Figure 7(d) that while the spectral density becomes higher with the increase of contact stiffness, the frequency characteristic of contact force remains the same in term of frequency peaks. Meanwhile, the PSDs in the cases element number change and sampling interval change are very similar. For further analysis of simulated contact forces, these consistencies of mean and PSD prove the model validity at high frequencies to a certain extent.

Table 1. Selected parameter values for model validation and other related parameters.

Parameter	Value
Contact stiffness (N/m)	For model validation: From 20,000 to 90,000 For further simulations: 50,000
Number of elements between adjacent droppers or dropper and registration point	For model validation: 18 and 36 For further simulations: 24
Sampling interval (m)	For model validation: 0.025 and 0.075 For further simulations: 0.05
Span length (m)	60
Dropper distribution	10 droppers evenly distributed in one span
Contact wire tension (kN)	10
Messenger wire tension (kN)	10.8
Stagger (m)	± 0.2
Operation speed (km/h)	120

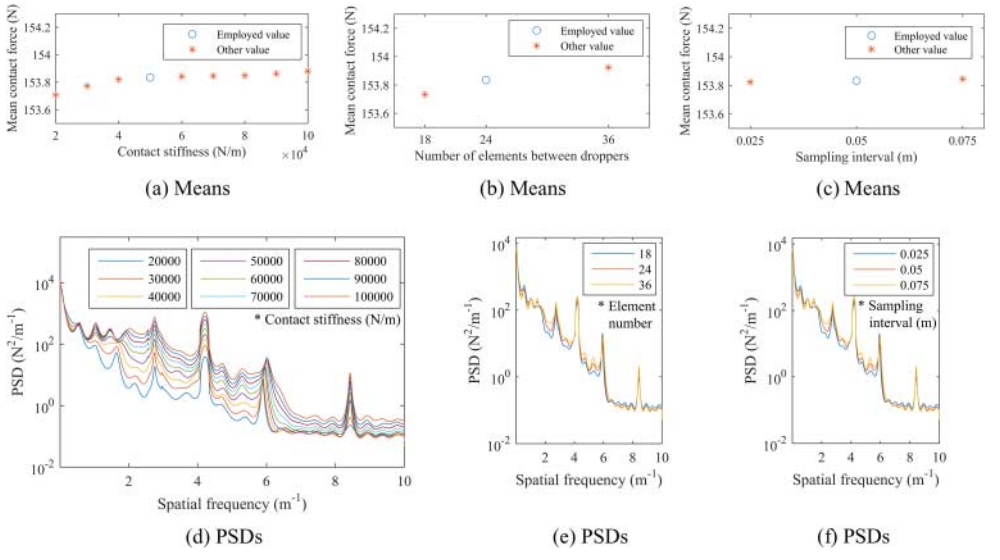

Figure 7. Comparisons of mean and PSD of contact force when the (a), (d) contact stiffness, (b), (e) element number and (c), (f) sampling interval are different.

5.2. Simulation of contact wire wear irregularity

The wire irregularity caused by geometric deformation that can lead to the variation of contact wire height is often the results of errors in dropper length or placement, wire tension and so on. Thus, it should be considered in the configuration stage of catenary modelling. However, the wear irregularity of contact wire basically differs from the irregularity caused by geometric deformation. Since it is irrespective to the initial configuration of catenary, it can be neglected in the configuration stage. Thus, the wire thickness loss can be simply included in the penalty function in Equation (12) as a modification to the penetration depth [9,31]

$$\begin{aligned} F_c(x,t) &= K_c(u_p(t) - u_c(t) - z_w(x)) \quad u_p(t) - u_c(t) - z_w(x) \geq 0, \\ F_c(x,t) &= 0 \quad u_p(t) - u_c(t) - z_w(x) < 0, \end{aligned} \tag{14}$$

where $z_w(x)$ is the contact wire thickness loss at position x.

To simulate the actual growth of contact wire wear irregularity, the average thickness loss reflected by the data depicted in Figure 1(a) is employed. Correspondingly, the mutual influences of wear growth and pantograph–catenary interaction on each other can be investigated. Both local and distributed irregularities are considered for simulation. In the case of local wear irregularity, the severe thickness loss of contact wire located at the beginning of the data set is selected as the input. As a singular irregularity, it includes the thickness loss with a total contact wire length of 7 m as shown in Figure 8. In the interaction model, the thickness loss from each year is equivalently added to the penalty function, simulating the local wire wear locating at the 7th span where the influence of boundary effect is negligible in the 14-span catenary model. For the complex distributed wear irregularity, the entire data series of contact wire thickness loss from year 1 to year 4 are added to the interaction model in the same manner. It simulates a 10-span section of contact wire with actual

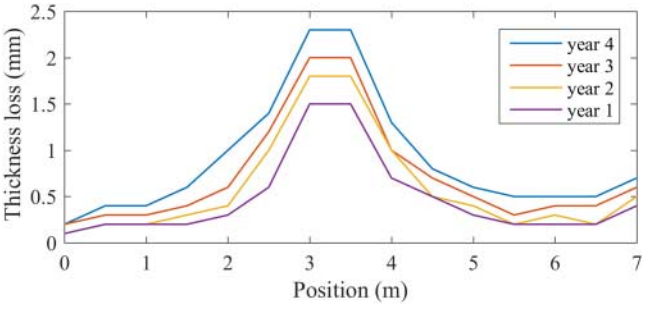

Figure 8. Growth of singular local wear irregularity employed in simulations.

wear irregularity locating at the middle of the catenary model, that is, from the 3rd span to the 12th span. Since the sampling interval is set to 0.05 m in simulation, the thickness loss data is interpolated by linear interpolation to form smooth wear irregularities that will be reflected in the contact force.

6. Wear irregularity and pantograph–catenary contact force

6.1. Influence of singular local wear irregularity

Simulations are carried out with a constant operation speed that is the average commercial speed of 120 km/h for the pantograph motion. To study the relationship between contact wire wear irregularity and pantograph–catenary interaction, the contact force between pantograph and catenary is selected as the reflection of the interaction. The contact force simulated without intentionally adding wear irregularity to the contact wire is regarded as the reference of normal contact force. Generic technical standards suggest that, before using the contact force to evaluate the pantograph–catenary interaction, the contact force should be filtered by a low-pass filter with 20 Hz cut-off frequency. But, recent advances realised the limitations of this frequency boundary and suggested a boundary up to 200 Hz to preserve useful information in the contact force concerning the condition monitoring of catenary [32,33]. In the case of contact wire wear, the wavelength of distributed irregularity or the length of local irregularity are likely to be shorter than those of geometric deformation, which consequently requires a high sampling frequency to be observable from measurements. Therefore, the sampling interval in simulations is set to be 0.05 m that is equivalent to over 600 Hz sampling frequency under the 120 km/h operation speed, as an attempt to discover new insights in a higher frequency band.

Figure 9 depicts the force differences between the contact forces simulated under the growing local wear irregularity described in the previous section and the reference contact force. The location of the local wear irregularity is indicated by the interval between the dashed lines. It can be seen that, starting from the origin of the local irregularity located at 420 m, the contact forces deviate from the reference one due to the influence of the irregularity. The influence continues after the pantograph passed through the irregularity. The overall amplitude of the caused deviation is higher when the irregularity is severer with higher thickness loss every year. As statistically shown in Table 2, the thickness losses result in small decreases of the average contact force and increases of SD in the 2-span duration

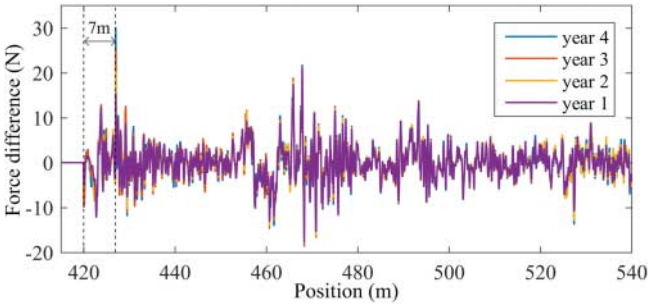

Figure 9. Contact force differences under singular local wear irregularity comparing with the reference force.

from 420 to 540 m. This is because the thickness loss actually reduces the penetration depth as given in Equation (14), but also elevates the vibration between the pantograph and contact wire. Meanwhile, the variation in the SD of contact force difference is significantly higher comparing with that of the average contact force difference. Although the variation in this case of singular irregularity only has a small impact on the overall contact force, the impact will be much higher when multiple local irregularities exist and their impacts accumulate to a considerable change of the contact force statistic.

In the frequency domain, it can be seen from Figure 10(a) that the PSDs of contact forces under local irregularities have very small variations comparing with the PSD of contact force without irregularity. In the enlarged low-frequency Region 1, the first two frequency peaks respectively locate at around 5.5 and 3.2 m wavelength, which corresponds to the first two peaks depicted in Figure 4 as a result of contact force acting on the contact wire. Although the impact of the singular local wear irregularity is limited, it still slightly increases the energy of the dominant frequency peaks. In the enlarged high-frequency Region 2, the changes of high-frequency peaks are considerable. It indicates that the singular irregularity induces more intense high-frequency vibration as the irregularity grows. From the PSDs of contact force differences depicted in Figure 10(b), influences of the singular irregularity on contact force are easily observable. While the overall level of spectrum is increasing with the yearly irregularity growth, the spectrum difference in the high-frequency range is relatively more significant than that in the low-frequency range. This reflects that the singular irregularity can contribute to the vibration of pantograph–catenary interaction, especially at high-frequency ranges, despite its limited alteration in the penetration depth of contact.

Table 2. Comparisons of the mean and SD of contact forces and contact force differences under singular local wear irregularity.

	Contact force (N)		Contact force difference (N)	
Condition	Mean	SD	Mean	SD
Reference	153.3231	27.1895	0	0
Year 1	153.3222	27.2492	−0.0009	2.6474
Year 2	153.3215	27.2752	−0.0016	2.7735
Year 3	153.3189	27.2944	−0.0043	2.8872
Year 4	153.3135	27.3099	−0.0096	2.9884

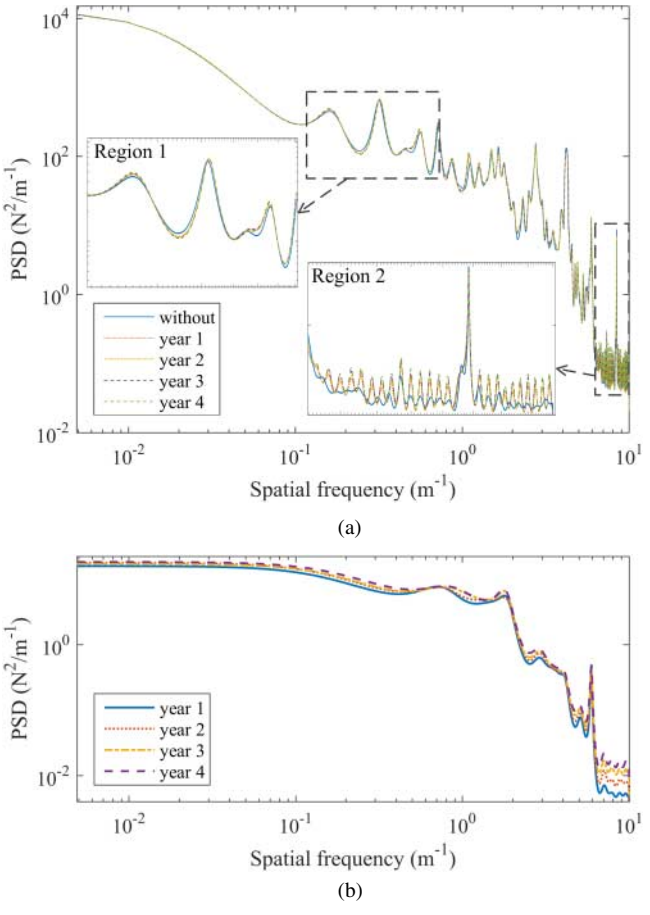

Figure 10. PSD Comparisons of (a) contact forces and (b) contact force differences under local wear irregularities.

The frequency variation of contact forces along the longitudinal position is depicted in Figure 11 with TFRs based on wavelet transform. The interval between the dashed lines indicates the location of the singular irregularity. A narrow position window from 419 to 436 m near the location of the singular irregularity is used to compute the TFRs. This is to make the small frequency variation caused by the singular irregularity observable. Taking the TFR of normal contact force on the left as the reference, two types of frequency variation can be identified as the impact of the singular irregularity on the contact force. The first one is located at the end of the singular irregularity around 4.4 m^{-1} spatial frequency. It is the reflection of the abnormally high contact force corresponding to the high contact force difference located at the end of the singular irregularity as depicted in Figure 9. It also corresponds to the frequency peak of PSDs located at around 4.4 m^{-1} spatial frequency outside the Region 2 depicted in Figure 10(a). This emerging frequency can be considered as a new indicator to identify local wear irregularity from the TFR of contact force, but it is only applicable when the measurement frequency for contact force is sufficiently high. The second one is located at around 0.4 m^{-1} where the similar directional

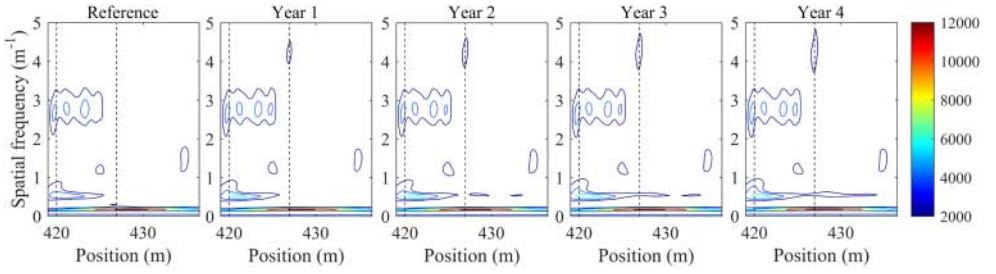

Figure 11. TFR Comparisons of contact forces with and without local contact wire wear irregularities.

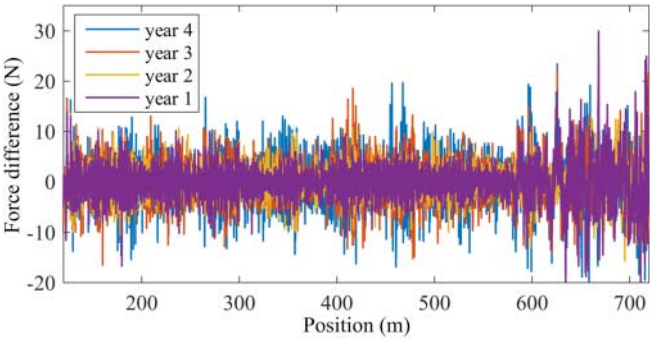

Figure 12. Contact force differences under complex distributed wear irregularity comparing with the reference force.

property is found in the evolvement of contact force as the effect of pantograph passage. In the reference TFR, there is already an energy peak at 420 m that is presumably due to the fixing of registration arm. When the singular irregularity is added, the energy is growing and also expanding in the longitudinal direction, that is, the running direction of pantograph with the yearly growing irregularity. Since the singular irregularity is only alteration in the simulation, this pattern of change can also be identified as the result of the singular irregularity. Therefore, with multiple local wear irregularities existing along the contact wire, the pattern will aggregate and leading to the formation of contact wire wear with the same directional property as previously discussed.

6.2. *Influence of complex distributed wear irregularity*

The added complex wear irregularity is the combination of multiple local and distributed irregularities existed along the 10 spans long catenary in real life. Presumably, it should have a higher impact on the pantograph–catenary interaction than in the case of singular local irregularity. Through simulations according to previous description, the contact force under complex irregularities is acquired and the force differences with the reference contact force are depicted in Figure 12. With some exceptional sample points, the force difference is generally higher as the contact wire wear becomes severer. Also, the force variation is abnormally drastic after 600 m due to the boundary effect of simulation model. From the statistics listed in Table 3, it can be seen that while the mean of contact force still remains

Table 3. Comparisons of the mean and SD of contact forces and contact force differences under complex distributed wear irregularity.

	Contact force (N)		Contact force difference (N)	
Condition	Mean	SD	Mean	SD
Reference	153.8336	27.6230	0	0
Year 1	153.7214	29.2038	−0.1122	5.0848
Year 2	153.7056	29.5203	−0.1280	5.6087
Year 3	153.6803	29.7413	−0.1533	6.0639
Year 4	153.6266	29.9924	−0.2070	6.5194

close, the SD of contact force increases significantly by at least 5.7% comparing with the 0.4% when only the singular irregularity is added. For the same cause, the mean and SD of the contact force difference also change considerably.

The impact of complex wear irregularity can also be reflected by the PSD of contact forces. Figure 13(a,b), respectively depict the PSDs of the simulated contact forces and contact force differences against the reference. Comparing Figure 13(a) with Figure 10(a), it can be seen that the spectrum difference caused by the complex irregularity becomes more significant than that of the singular irregularity. Particularly, in the high-frequency range shown in Region 1, the additional spectrum rise and decline caused by the added irregularity indicate that the contact force fluctuation in the dominant frequency band is influenced by the irregularity. It is mainly because the wear irregularity is the result of actual pantograph–catenary interaction and thus shares the same frequency pattern that is related to the catenary structure, which correspondingly excites the vibration of catenary. The PSDs of contact force differences in Figure 13(b) also shows the rise of spectral density is shifting to higher frequencies comparing with those in Figure 10(b). However, these changes in PSDs are still small and difficult to be quantified concerning the awareness of the existence of wear irregularities. The results suggest that the PSD of contact force can only reveal limited information on the contact wire wear irregularity, entailing the needs of TFR for the complete characterisation, or even the detection and localisation of wear irregularity.

The TFR of contact forces from the 10-span catenary can reveal the distribution of frequency variation caused by the complex wear irregularity along the contact wire. Because the impact of wear irregularity compared with the overall contact force is relatively small in amplitude, instead of computing the TFRs of contact force, TFRs of the contact force differences against the reference force are adopted and depicted in Figure 14 for concise comparisons. In each TFR, three vertical dashed lines indicate the middle position of three severely worn wire segments that stand out in the data depicted in Figure 1(a), which are located at 3.5, 146 and 261 m, respectively. In the catenary model, the corresponding positions are at 123.5, 266 and 381 m, respectively, with two additional spans at the front. It can be clearly seen that the impact of complex irregularity is increasing with the deterioration of wear irregularity mostly in low-frequency range. By the year 3 and 4, there is a periodical pattern showing that the contact force is additionally excited at about every 60 m in higher frequency range, which accelerates the formation of severe local irregularity for contact wire at the registration arm. Meanwhile, in these TFRs with a wide time window, the effects of local irregularities whose position are indicated by dashed lines cannot be fully observed. Only the first and severest one at the beginning shows certain indication

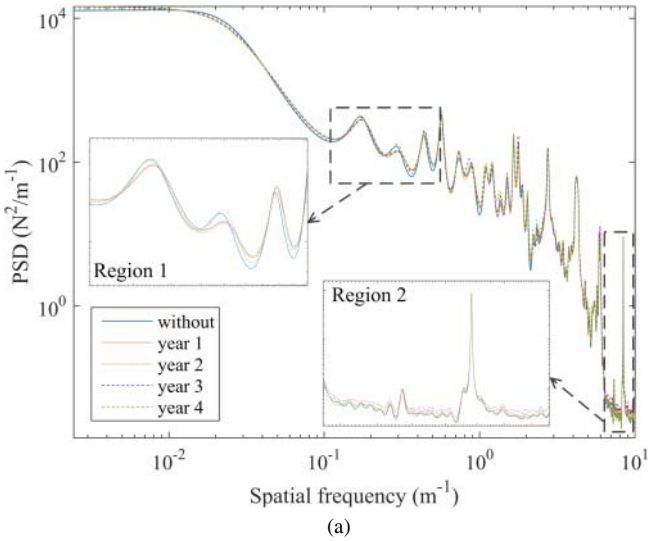

(a)

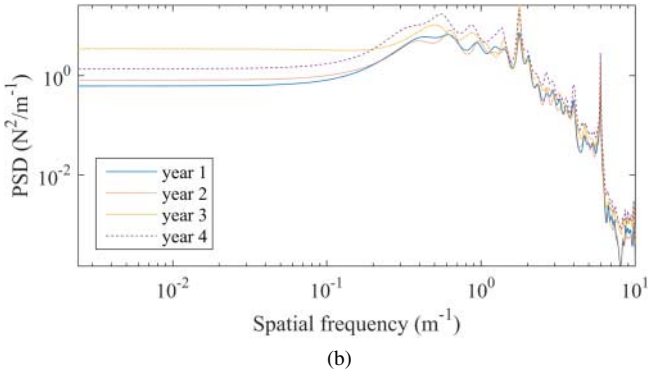

(b)

Figure 13. PSD comparisons of (a) contact forces and (b) contact force differences under local wear irregularities.

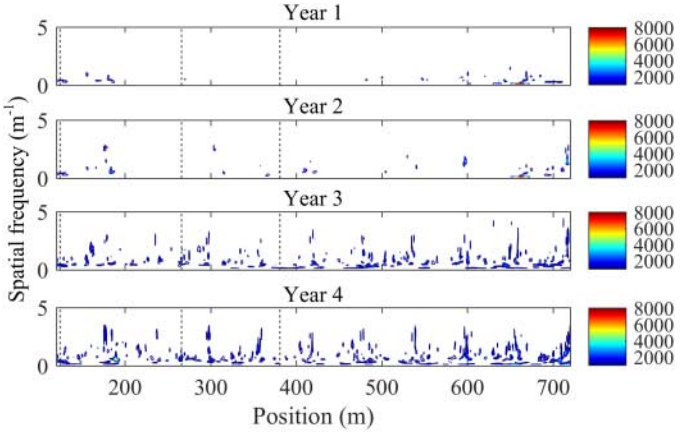

Figure 14. TFR comparisons of contact force differences under complex distributed wear irregularities.

of frequency variation at about 0.4 m^{-1} spatial frequency that is in accordance with the variation illustrated in Figure 11.

For the thorough observation of local irregularities among the complex irregularity, Figure 15 depicts the TFRs of local contact forces around the midpoints of three local irregularities indicated by dashed lines. Impacts of the local irregularities on the contact force shows similar but also different representation due to their distinguishing location in catenary structure and amplitude in thickness loss. From Figure 15(a), it can be seen that the first local irregularity, as the severest one, shows very similar representation comparing with when it is solely added in the catenary model as depicted in Figure 11. There are emerging frequency components identified around 0.4 and 4.4 m^{-1}, which are expanding with the grow of thickness loss. It is worth noting that in the TFR of reference contact force, there is originally a frequency component around 3 m^{-1} that is caused by the fixing of registration arm at 120 m. For the second and third local irregularities that are not near the fixing points, there is naturally no such kind of interference for irregularity identification. In Figure 15(b), the similar frequency variations can be found near the midpoint of the second irregularity comparing with those caused by the first one in Figure 15(a). Meanwhile, Figure 15(c) shows that the third one has relatively lower impact on the contact force than

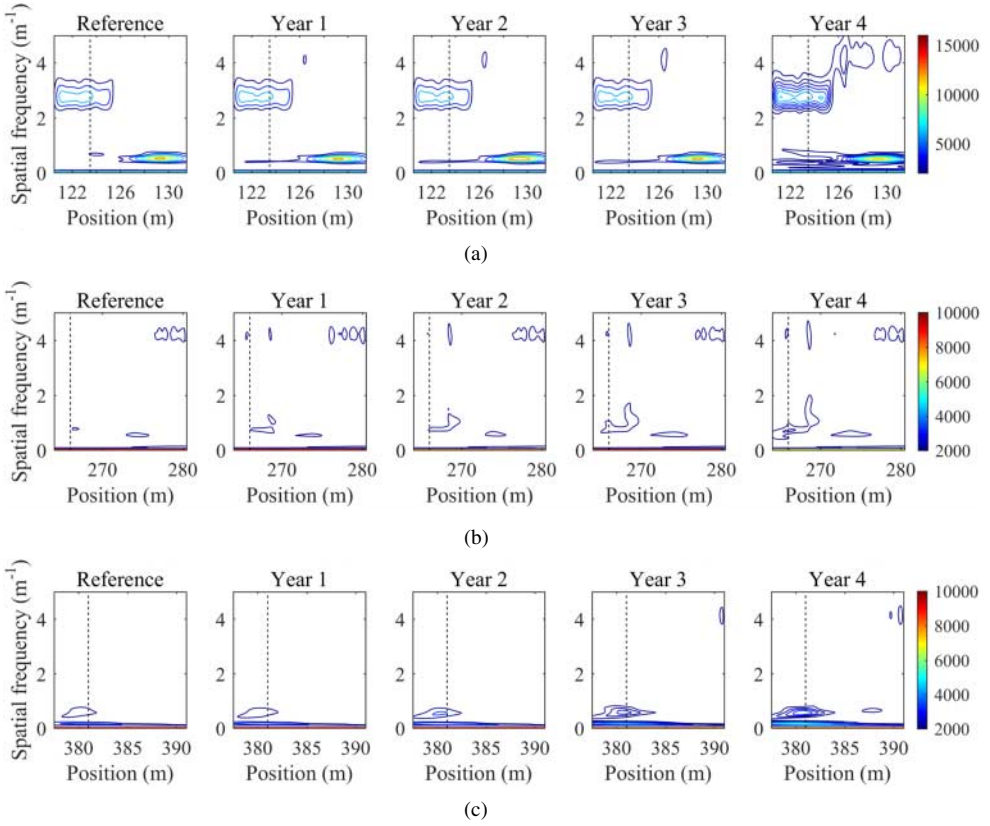

Figure 15. TFR comparisons of contact forces around the three local wear irregularities in (a), (b) and (c), respectively.

the first two with only the frequency variation around $0.4\,\mathrm{m}^{-1}$ identified. This is likely the result of a relatively low thickness loss.

From the above analyses on both singular and complex irregularities, it can be speculated that the reflection of local wear irregularities in the contact force requires a high measurement frequency to reveal. In the case of this paper, the indicative spatial frequency of $4.4\,\mathrm{m}^{-1}$ means that a sampling interval shorter than 0.23 m or frequency higher than 147 Hz is necessary.

6.3. From contact force to wear irregularity

The pantograph–catenary interaction not only suffers the impact caused by the wear irregularity of contact wire, but also contributes to the formation of the irregularity. The causes of contact wire wear mainly include sliding friction and electric corrosion [10–15]. In this paper, since the electrical aspect of wear formation is not considered, the growth of wire wear cannot be quantitatively estimated. However, based on the simulation results of pantograph–catenary contact force, the cause of wear evolvement can be qualitatively analysed, assuming that the friction coefficient is approximately constant. By comparing the simulated contact force and the corresponding wear growth over time, the pattern of wear irregularity evolvement can be partly identified and explained according to the variation of contact force simulated from the thickness loss measured in different year.

Concretely, the contact forces simulated under complex distributed wear irregularities in the previous section are adopted as the reflections of contact wire wear. For example, the contact force under the influence of thickness loss measured in year 1 can be associated with the growth of the thickness loss measured in year 2. To this end, the contact force $F_c(x,t)$ is firstly transformed using the threshold-based criterion as follows.

$$\begin{aligned} F_T(x,t) &= 1 \quad F_c(x,t) \geq \mathrm{mean}[F_c(x,t)] + 3 \cdot \mathrm{std}[F_c(x,t)], \\ F_T(x,t) &= 0 \quad F_c(x,t) < \mathrm{mean}[F_c(x,t)] + 3 \cdot \mathrm{std}[F_c(x,t)], \end{aligned} \tag{15}$$

where $\mathrm{mean}[F_c(x,t)]$ and $\mathrm{std}[F_c(x,t)]$ denote the mean and SD of contact force, respectively. The value 1 indicates the existences of abnormally high contact force that can leads to severe wear. Then, the measured minimum thickness of contact wire is employed to show the distribution of wear corresponding to the contact force. The thickness loss $L(x)$ from different year is normalised for comparisons with the transformed contact force.

$$L_N(x) = \frac{L(x) - \min[L(x)]}{\max[L(x)] - \min[L(x)]}. \tag{16}$$

The results of the qualitative comparison are depicted in Figure 16 by showing the normalised thickness loss from a certain year with the transformed contact force from the previous year. It can be seen that, from year 1 to year 3, most of the sample points of high contact force overlap with or locate close to the locations where severe thickness loss exists in year 2, 3 and 4, respectively. Since the contact force is theoretically proportional to the growth of thickness loss, the wear irregularity of contact wire thus increases year by year because of the abnormal contact forces. Also, the occurrence rate of high contact force,

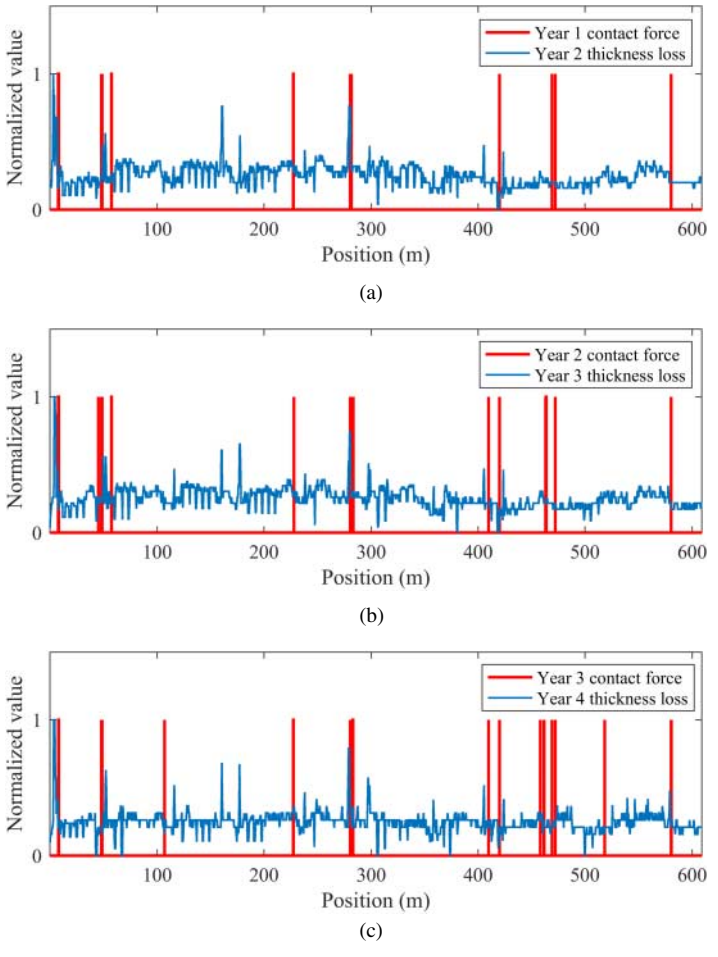

Figure 16. Comparisons between transformed contact force and normalised thickness loss. (a) Contact force simulated from year 1 and thickness loss measured in year 2. (b) Contact force simulated from year 2 and thickness loss measured in year 3. (c) Contact force simulated from year 3 and thickness loss measured in year 4.

namely the proportion of value 1 in the transformed contact force is 1.4%, 1.7% and 2.1% in year 1, 2 and 3, respectively. It means that the number of local wear irregularity on the contact wire is also increasing with the deterioration of contact force after every year. Meanwhile, some of the severe thickness loss appear not to be related to the contact force. This can be the results of electric corrosion, especially arcing effects that are not considered in this paper.

7. Conclusion

Making use of the annually recorded contact wire thickness data in past years, this paper presents the analysis of the evolvement of contact wire wear irregularity under daily operation. The evolvement itself and its influence on pantograph–catenary interaction are

studied by the PSD and wavelet transform with the help of FEM model. Based on the measured data from a local section of catenary and tailored pantograph–catenary numerical simulations, the following conclusions can be drawn.

(1) The formation of wear irregularity is mainly associated with the catenary structure. Thus, the wear irregularity contains structure wavelengths of catenary such as span and inter-dropper distance. The degree of irregularity in terms of these wavelengths will grow with time as the catenary structure is fixed. The contact wire segment located at the registration arm most likely suffers severe wear due to the high stiffness attributed to the fixing effect.
(2) The pattern of wear irregularity has a directional property that is depending on the common or dominant running direction of trains in the specific line. The wear irregularity of contact wire tends to spread toward the running direction with time. In this sense, the wire wear near the beginning of a tensioning section is generally severer than that near the end of the section.
(3) The contact wire wear irregularity has certain impact on pantograph–catenary contact force. While it can hardly influence the mean of pantograph–catenary contact force, it excites the vibration of pantograph and contact wire that results in the increasing SD of contact force, which will eventually exacerbate the degree of wear irregularity.
(4) It is possible to detect the contact wire wear irregularity by using the TFR of contact force to identify abnormal frequency peaks. In particular, local irregularities can be detected and localised in a short time window by emerging frequencies related to the local wear pattern and structural vibration frequency. The indicative frequency range is relatively high so that the commonly used upper measurement frequency bound of 20 Hz may be insufficient.

It should be noted that conclusion (3) and (4) concerning the contact force are drawn based on simulation results. They are essentially inferences to be realistically proven in the future based on dynamic measurements. Furthermore, contact wire thickness data from the same railway network with different operation condition and traffic density, or data from a different railway network should be comparatively investigated. Also, it is suggested that the measurement frequency band for whether the contact wire thickness or the contact force (or the pantograph head acceleration) should be expanded to enable the observation of short-wavelength wear irregularity and the corresponding high-frequency vibration response.

Acknowledgements

The authors would like to thank Harm Visser and Shaoguang Li for their help in the data acquisition of this paper.

Disclosure statement

No potential conflict of interest was reported by the authors.

Funding

This work was partly supported by the National Natural Science Foundation of China under grant U1434203, 51377136, 51405401, the Science and Technology Department of Sichuan Province under grant 2016TD0012, and the China Scholarship Council under grant 201507000029.

ORCID

Hongrui Wang http://orcid.org/0000-0001-7194-4728
Yang Song http://orcid.org/0000-0002-7699-5855

References

[1] Cats O, Yap M, van Oort N. Exposing the role of exposure: public transport network risk analysis. Transp Res A Policy Pract. 2016;88:1–14.
[2] Y Zhu, Goverde R. System-based vulnerability measures for railway systems. Proceedings of the 7th International Conference on Railway Operations Modelling and Analysis (IAROR): RailLille; 2017.
[3] Zhang W, Mei G, Zeng J. A study of pantograph/catenary system dynamics with influence of presag and irregularity of contact wire. Veh Syst Dyn. 2002;37:593–604.
[4] Nagasaka S, Aboshi M. Measurement and estimation of contact wire unevenness. Q Rep RTRI. 2004;45(2):86–91.
[5] Zhang W, Shen Z, Zeng J. Study on dynamics of coupled systems in high-speed trains. Veh Syst Dyn. 2013;51(7):966–1016.
[6] Collina A, Fossati F, Papi M, et al. Impact of overhead line irregularity on current collection and diagnostics based on the measurement of pantograph dynamics. Proc Inst Mech Eng F J Rail Rapid Transit. 2007;221(4):547–559.
[7] Zhang W, Mei G, Wu X, et al. Hybrid simulation of dynamics for the pantograph–catenary system. Veh Syst Dyn. 2002;38(6):393–414.
[8] Wang H, Liu Z, Song Y, et al. Detection of contact wire irregularities using a quadratic time-frequency representation of the pantograph–catenary contact force. IEEE Trans Instrum Meas. 2016;65(6):1385–1397.
[9] Vo Van O, Massat JP, Laurent C, et al. Introduction of variability into pantograph–catenary dynamic simulations. Veh Syst Dyn. 2014;52(10):1254–1269.
[10] Collina A, Melzi S, Facchinetti A. On the prediction of wear of contact wire in OHE lines: a proposed model. Veh Syst Dyn. 2002;37(sup1):579–592.
[11] Bucca G, Collina A. A procedure for the wear prediction of collector strip and contact wire in pantograph–catenary system. Wear. 2009;266(1):46–59.
[12] Yamashita C, Sugahara A. Wear modes of contact wire and contact strip under electric current condition. Q Rep RTRI. 2014;55(2):67–72.
[13] Nagasawa H, Kato K. Wear mechanism of copper alloy wire sliding against iron-base strip under electric current. Wear. 1998;216(2):179–183.
[14] Zhao H, Barber GC, Liu J. Friction and wear in high speed sliding with and without electrical current. Wear. 2001;249(5):409–414.
[15] Ding T, Chen GX, Bu J, et al. Effect of temperature and arc discharge on friction and wear behaviours of carbon strip/copper contact wire in pantograph–catenary systems. Wear. 2011;271(9):1629–1636.
[16] Kim J, Chae H, Park B, et al. State sensitivity analysis of the pantograph system for a high-speed rail vehicle considering span length and static uplift force. J Sound Vib. 2007;303(3):405–427.
[17] Zhang W, Liu Y, Mei G. Evaluation of the coupled dynamical response of a pantograph–catenary system: contact force and stresses. Veh Syst Dyn. 2006;44(8):645–658.
[18] Nåvik P, Rønnquist A, Stichel S. The use of dynamic response to evaluate and improve the optimization of existing soft railway catenary systems for higher speeds. Proc Inst Mech Eng F J Rail Rapid Transit. 2016;230(4):1388–1396.

[19] Rønnquist A, Nåvik P. Dynamic assessment of existing soft catenary systems using modal analysis to explore higher train velocities: a case study of a Norwegian contact line system. Veh Syst Dyn. 2015;53(6):756–774.
[20] Kudo S, Honda S, Ikeda M. Contact force signal analysis of current collecting with bispectrum and wavelet. Proceedings of the 41st SICE Annual Conference, Vol. 4. IEEE; 2002, p. 2478–2482.
[21] Mallat S, Hwang WL. Singularity detection and processing with wavelets. IEEE Trans Inf Theory. 1992;38(2):617–643.
[22] Kusumi S, Fukutani T, Nezu K. Diagnosis of overhead contact line based on contact force. Q Rep RTRI. 2006;47(1):39–45.
[23] Stoica P, Moses RL. Introduction to spectral analysis. Upper Saddle River: Prentice Hall; 1997.
[24] Akaike H. Power spectrum estimation through autoregressive model fitting. Ann Inst Stat Math. 1969;21(1):407–419.
[25] Akaike H. An information criterion (AIC). Math Sci. 1976;14(153):5–9.
[26] Mallat S. A wavelet tour of signal processing. 2nd ed. London: Academic Press; 1999.
[27] Liu Z, Wang H, Dollevoet R, et al. Ensemble EMD-based automatic extraction of the catenary structure wavelength from the pantograph–catenary contact force. IEEE Trans Instrum Meas. 2016;65(10):2272–2283.
[28] Bruni S, Ambrosio J, Carnicero A, et al. The results of the pantograph–catenary interaction benchmark. Veh Syst Dyn. 2015;53(3):412–435.
[29] Song Y, Liu Z, Wang H, et al. Nonlinear modelling of high-speed catenary based on analytical expressions of cable and truss elements. Veh Syst Dyn. 2015;53(10):1455–1479.
[30] European Committee for Electrotechnical Standardization EN 50318. Railway applications – current collection systems – validation of simulation of the dynamic interaction between pantograph and overhead contact line. Brussels: European Standards; 2002.
[31] Song D, Jiang Y, Zhang W. Dynamic performance of a pantograph–catenary system with consideration of the contact surface. Proc Inst Mech Eng F J Rail Rapid Transit. 2016. DOI:10.1177/0954409716664934.
[32] Boffi P, Cattaneo G, Amoriello L, et al. Optical fiber sensors to measure collector performance in the pantograph–catenary interaction. IEEE Sens J. 2009;9(6):635–640.
[33] Carnevale M, Collina A. Processing of collector acceleration data for condition-based monitoring of overhead lines. Proc Inst Mech Eng F J Rail Rapid Transit. 2016;230(2):472–485.